ISSN 2411-3336; e-ISSN 2541-9404

JOURNAL OF MINING INSTITUTE

Zapiski Gornogo instituta

Journal homepage: pmi.spmi.ru

Research article

Acoustic emission criteria for analyzing the process of rock destruction and evaluating the formation of fractured reservoirs at great depths

Vladimir L. Trushko✉, Aleksandr O. Rozanov, Malik M. Saitgaleev, Dmitrii N. Petrov, Mikhail D. Ilinov, Daniil A. Karmanskii, Aleksandr A. Selikhov

Empress Catherine II Saint Petersburg Mining University, Saint Petersburg, Russia

***How to cite this article*:** Trushko V.L., Rozanov A.O., Saitgaleev M.M., Petrov D.N., Ilinov M.D., Karmanskii D.A., Selikhov A.A. Acoustic emission criteria for analyzing the process of rock destruction and evaluating the formation of fractured reservoirs at great depths. Journal of Mining Institute. 2024. Vol. 269, p. 848-858.

Abstract. In order to study the mechanism of destruction of rocks of various genesis and the formation of fractured reservoirs at great depths, laboratory studies of rock samples in the loading conditions of comprehensive pressure with registration of acoustic emission (AE) and parameters of the process of changing the strength and deformation properties of samples were carried out. The spatial distributions of the hypocenters of AE events for each sample were investigated. By the nature of the distributions, the fracture geometry is described, then visually compared with the position of the formed macrofractures in the samples as a result of the tests. The time trends of the amplitude distribution *b*, set by the Guttenberg – Richter law, were calculated, which were compared with the loading curves and trends of the calculated AE activity. Based on the analysis of the AE process for three types of rocks – igneous (urtites), metamorphic (apatite-nepheline ores), and sedimentary (limestones) – parameterization of acoustic emission was carried out to determine the features of the deformation process and related dilatancy. As a result, three types of destruction of samples were identified, their geometry and changes in strength and seismic criteria were established.

***Keywords*:** acoustic emission; physical-mechanical properties; *b*-factor; destruction criteria; dilatancy; distribution of hypocenters

Funding. The work was carried out within the framework of the state task FSRW-2024-0008 “Investigation of thermodynamic processes of the Earth from the perspective of the genesis of hydrocarbons at deep depths”.

Received: 09.09.2024 ***Accepted: 05.11.2024*** ***Online: 12.11.2024*** ***Published: 12.11.2024***

Introduction. The study of the processes of rock destruction of various genesis and the mechanism of formation of fractured reservoirs at great depths [1-3] is relevant for understanding the formation of natural reservoirs and multilevel hydrocarbon deposits under extreme thermobaric conditions [4, 5]. The destruction of rocks and the phenomenon of dilatancy are studied by various methods [6-10], which revealed a complex process of development of critical deformations in defective structures [11-14], including a plastic stage and brittle fracture. Laboratory modeling of the disturbance of rock salt and Cambrian clay when loading samples before moving to the extreme part of the stress – strain diagram and subsequent creep tests of disturbed and undisturbed samples showed a significant decrease in creep deformations in disturbed rocks and a decrease in their contribution to the further destruction process [15-17].

In consolidated rocks, the dilatancy property manifests itself through the formation of a microcrack zone, which includes a fracture preparation zone and is characterized by an intense interaction of separation microcracks determined by the size of mineral grains, as a result of which a macrofracture is formed [18, 19]. Studies [20-22] of the process of destruction of igneous (granites) and sedimentary (sandstones) rocks with AE registration give a general idea of the development of fracturing in rocks under load [23-25].

This is an open access article under the CC BY 4.0 license

Initially, microcracks of break-off are formed without significant interaction with each other, characterized by a spatial distribution unrelated to the trajectory and location of the future macrofracture. As the load approaches the tensile strength, the formation of the embryo of a future macrofracture begins, when several microcracks of break-off interact and strengthen the opening of each other. They form a zone of the destruction process – an area of microcracks located close to each other. In a critically loaded rock, the stress field created by tensile forces in microcracks provokes the interaction of cracks and causes unstable propagation of these cracks into an intact area of the rock. As the size of the fracture zone increases, its central part is weakened by shear deformations, and as a result, instability occurs, which spreads along the trail of the developing fracture zone. Stress fields related to shear along the break enhance the opening of microcracks in the fracture zone, thereby converting the process into an avalanche-like formation of microcracks and a transition to macrodestruction.

Thus, what is common to the model of brittle fracture of consolidated rocks is that the formation of a macrofracture occurs as a result of the close interaction of several microcracks when a critical density is reached. In this case, the break propagates in a plane forming an angle $\beta = 20\text{-}30°$ to the axis of the maximum compression stress σ_1 [20] in accordance with the analytically described stress fields of expanding microcracks [26].

The germination of expanding microcracks in brittle rocks, which are subjected to comprehensive compression, is caused by the action of inhomogeneous stress, depending on the structural features of the rock. Such structural features include the size of mineral grains, imperfect contacts of grain boundaries, differences in elastic modulus of composite minerals, intracrystalline defects, as well as shear deformations along grain boundaries. In [27], the distribution of microcracks in physical and numerical modeling in granite is considered, where, as a result of destruction, a rock mass of communicating microcracks and many isolated ones are revealed. Based on the identity of the image of this distribution to the calculated geometries of the hypocenters of AE events for igneous rocks, the definition of the microcrack zone is formulated. The microcrack zone corresponds to the volume of the rock mass of communicating (presumably) cracks, which is characterized by a density of AE events of at least 0.0125 events/mm^3 according to the calculation method used in the work.

The purpose of this work is to parameterize the fracture according to four criteria – fracture geometry, tensile strength, amplitude distribution, and AE activity. Parameterization was carried out based on the results of analysis of laboratory tests of the destruction of two samples of igneous (urtites), two metamorphic (apatite-nepheline ores) and two sedimentary rocks (limestones).

Methods. Magmatic rocks were selected for laboratory studies of the deformation process: coarse-grained massive urtites with a grain size of 5-10 mm (Khibinskoye deposit), metamorphic rocks represented by apatite-nepheline ores of poor and rich zones, composed of a fine-grained aggregate of sugar-like apatite with a size of 2-1 mm (Khibinskoye deposit) [28], and sedimentary rocks – hidden fine-grained gray limestones (core material of well 3-Nerutynskaya) (Table 1).

Table 1

Rock structure

Origin	Sample	Rock	Structure
Magmatic	N1’	Massive urtites	Coarse-grained (grain size 5-10 mm)
	N8	Massive urtites	Coarse-grained (grain size 5-10 mm)
Metamorphic	N1	Apatite-nepheline ore of the poor zone	Fine-grained (grain size 2-1 mm)
	N2	Apatite-nepheline ore of the rich zone	Fine-grained (grain size 2-1 mm)
Sedimentary	DP 22-2	Grey limestone	Hidden fine-gained
	DP 21-2		

This is an open access article under the CC BY 4.0 license

Journal of Mining Institute. 2024. Vol. 269. P. 848-858
© Vladimir L. Trushko, Aleksandr O. Rozanov, Malik M. Saitgaleev, Dmitrii N. Petrov, Mikhail D. Ilinov, Daniil A. Karmanskii, Aleksandr A. Selikhov, 2024

Studies of the behavior of rock samples under volumetric stress conditions were carried out on the MTS 815 servo-hydraulic pressing unit with the Milne DAQ acoustic emission system integrated into it (An Itasca International Company, UK). The technical characteristics of the MTS 815 unit make it possible to create lateral and pore pressure in the range from 0 to 80 MPa and an axial load on the sample up to 4600 kN. This system can simulate the stress state of a rock mass up to depths of 5-6 km. Structurally, the MTS 815 unit includes a power frame, a triaxial compression chamber, lateral and pore pressure amplifiers, controllers and a software package for automatic control of the loading mode, collecting and processing information from the force sensor and longitudinal and transverse strain sensors.

AE signals were recorded by the Milne DAQ data acquisition system in trigger mode. The main parameters of the launch and registration were controlled using the Milne Leach software module: the signal digitization frequency was 10 MHz; the number of samples for each signal was 2048 samples; the dynamic range was 5 V; the launch threshold for each channel was 80-100 mV.

The test preparation process consisted of sealing the side and end surfaces of the sample using a rubber shell. Acoustic emission sensors were placed on the side surface of the sample. The sample was placed in a triaxial compression chamber, in which a lateral pressure of σ_3 was created by mineral oil, corresponding to the simulated depths. Then the sample was loaded with an axial load σ_1. The loading was performed in the mode of a given deformation rate equal to 0.01 mm/min. The constant loading speed was ensured by the automatic press control system. During the experiment, the readings of the force sensor and sensors of longitudinal and transverse deformation with a frequency of 1 Hz were recorded, according to which graphs of changes in longitudinal, radial and volumetric deformations from the stress value were plotted.

The tensile strength under volumetric compression and a given value of lateral pressure for each sample is calculated using the formula $\sigma_c^v = \sigma_c^p + \sigma_3$, where σ_c^p – tensile strength under volumetric compression without taking into account the value of lateral pressure σ_3.

Table 2 provides information on the strength and deformation properties of the studied rock samples.

Table 2

Physical and mechanical properties of rocks

Type of rock	Density, kg/m^3	Strength, MPa		Coupling, MPa *	The angle of internal friction, degree*	Modulus of elasticity, GPa	Poisson's ratio
		With uniaxial compression	In tension				
Igneous (urtites)	2640	160.2	15.1	38.7	50.9	58.7	0.06
Metamorphic (rich ores)	3170	63.6	8.15	17.0	51.5	37.3	0.14
Metamorphic (poor ores)	2950	119.3	11.5	25,9	53.5	56.5	0.13
Sedimentary (limestone)	2571	153.2	14.8	41.7	37.1	69.5	0.32

* The parameters are determined based on the results of tests with uniaxial and volumetric compression.

The coordinates of the AE hypocenters were calculated using the commercial software ASC InSite Seismic Processor (An Itasca International Company, UK). The wave speeds in the location algorithm for urtites were set equal to V_p = 4767 m/s, V_s = 3150 m/s, speeds for ores – V_p = 3517 m/s, V_s = 1691 m/s. The wave speeds were measured by ultrasound before testing each sample. To locate the sources, 12 AE sensors with a contact pad with a diameter of 8 mm and a piezoelectric element diameter of 5 mm were used. The automatic determination of the time of the first entry was carried out by the RMS auto-picking function built into the InSite Seismic Processor.

For spatial parameterization of the deformation process, the density of AE events was calculated, according to the distribution of which in the sample volume the ratio of the maximum width of the microcrack zone to the length of the main crack was estimated, as well as the angle of inclination β of the main crack in accordance with the model [20]. The cross-sectional plane of the sample for the analysis of the microcrack zone was selected corresponding to the maximum density values.

This is an open access article under the CC BY 4.0 license

To parameterize the deformation process over time, the *b*-factor and AE activity were used; the *b*-factor was determined as a coefficient in the Guttenberg – Richter amplitude distribution formula [29-31]. This parameter characterizes the inverse of the probability of occurrence of high amplitude AE events, i.e. the value of *b* decreases with an increase in the number of high amplitude events. Thus, the *b*-factor corresponds to the scale of the energy emitted during a certain time interval of the test. In this paper, the analysis of the *b*-factor was carried out for an interval of significantly inelastic behavior of samples near the limiting stresses.

When parameterizing AE activity, the calculation of an approximation curve in the form of an exponent was used for a section of the activity trend corresponding to the stage of irreversible deformations, according to the formula

$$Y = C \exp(\alpha t),$$

where Y – approximate value of AE activity; C – scaling factor; α – exponent coefficient; t – the current time of the test.

The exponent coefficient characterizes the rate of increase in AE activity – the higher the value α, the faster the number of events per unit of time increases in the process of acoustic emission.

The *b*-factor calculation took into account the registration channel corresponding to the maximum amplitude signal for each AE event. To construct trends of the *b*-factor and AE activity, the method of a sliding time window of variable duration was used, which consistently moved along the time axis of each test. The window duration was chosen in such a way as to provide sufficient trend resolution and statistically significant estimates of the *b*-factor and AE activity. The calculation of the *b*-factor and AE activity was performed using a computer application developed by the authors of the article.

To illustrate the energy of AE events on the distribution of AE hypocenters, the magnitude values corresponding to the color diagrams for each sample were displayed. The magnitude was determined using the InSite Seismic Processor's built-in function for each location event as the logarithm of the average number of sensors of the product of the standard deviation of each event signal by the distance between the corresponding sensor and the event source.

Discussion of the results. The results of the analysis of the spatial distribution of AE hypocenters for igneous and metamorphic rocks are presented in the form of a comparison of the coordinates of AE events, event density distributions and photographs of samples after testing with a visible main crack. Figure 1 shows the AE hypocenters and their density distributions in accordance with the AE magnitude scale for igneous rock samples (urtites with a tensile strength of 523 and 463 MPa). It can be seen that diagonal macrofractures formed in both samples as a result of the final stage of destruction. Moreover, the most symmetrical shape of the microcrack zone is observed in a sample with a tensile strength of 463 MPa, which is consistent with the one obtained for granite in [27]. The angles of inclination β of the fractures for the samples are 22.32 and 20.44°, which satisfies the range predicted in [20] for the mechanism of brittle fracture through the militancy process of formation of a rock mass of layered microfractures of separation and concomitant shear deformation.

Figures 2 and 3 present the results of the analysis of the spatial distribution of AE hypocenters for samples of metamorphic rocks – ores of the poor zone with a tensile strength of 520 MPa (Fig.2) and ores of the rich zone with a tensile strength of 208 MPa (Fig.3). The poor zone ore sample is characterized by a diagonal type of macrofracture with an angle of 21.23°, which corresponds to the range of brittle fracture [20]. But, unlike urtites, there is a significant spatial localization of the process through the formation of two distinct clusters (Fig.2), in which the density of AE events increases almost twice as compared with urtites. At the same time, the width of the microcrack zone becomes significantly smaller compared to urtites, which affects a decrease in the ratio of the width of the zone to the length of the macrofracture (from 0.329 on average for urtites to 0.223 for the ore of the poor zone). This is consistent with the decrease in the width of the fracture preparation zone found in [32] with a decrease in the size of the mineral grains of the rock.

This is an open access article under the CC BY 4.0 license

© Vladimir L. Trushko, Aleksandr O. Rozanov, Malik M. Saitgaleev, Dmitrii N. Petrov, Mikhail D. Ilinov, Daniil A. Karmanskii, Aleksandr A. Selikhov, 2024

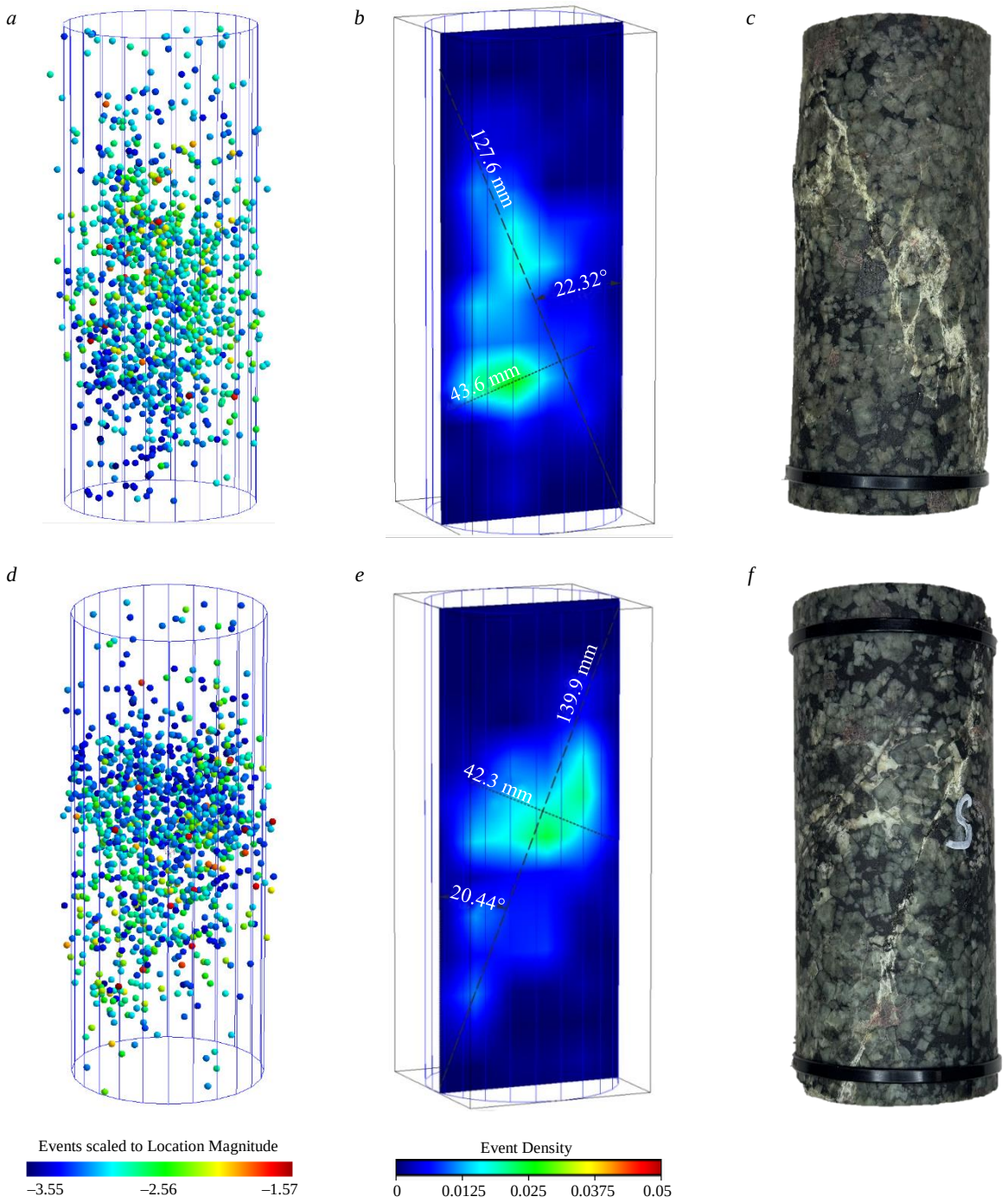


Fig.1. Analysis of the microcrack zone for igneous rocks (urtite sample with a tensile strength of 523 MPa (*a-c*) and 463 MPa (*d-f*): *a*, *d* – distribution of hypocenters of AE events; *b*, *e* – density of AE events; *c*, *f* – samples after testing with a diagonal main crack

The following main conclusion can be drawn regarding the described samples. A brittle fracture mechanism dominates in urtites and poor ores, while spatial localization and narrowing of the microcrack zone are manifested in the ore sample of the poor zone compared to urtites. At the same time, the *b*-factor and the coefficient of the exponent of AE activity α (hereinafter the exp-factor) grow from urtites to poor ores (Table 3). This fact indicates a decrease in the size of cracks in ores compared with urtites and, as a result, the localization of the AE process in time and space – an increase in the rate of formation of new cracks due to a closer location. The conclusion about the decrease in crack sizes with an increase in the *b*-factor is based on the theory outlined in [33].

This is an open access article under the CC BY 4.0 license

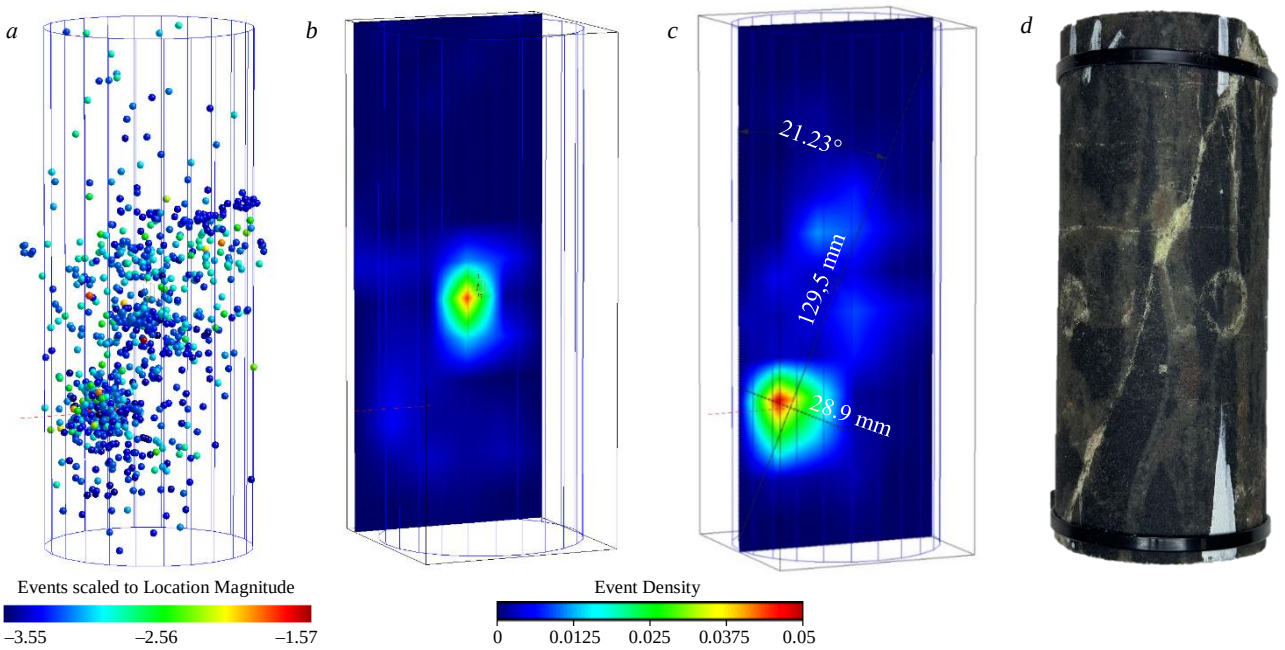


Fig.2. Analysis of the microcrack zone for metamorphic rocks (a sample of a poor zone ore with a tensile strength of 520 MPa): *a* – distribution of hypocenters of AE events; *b* – density of AE events for the first cluster; *c* – density of AE events for the second cluster; *d* – sample after testing with a diagonal main crack

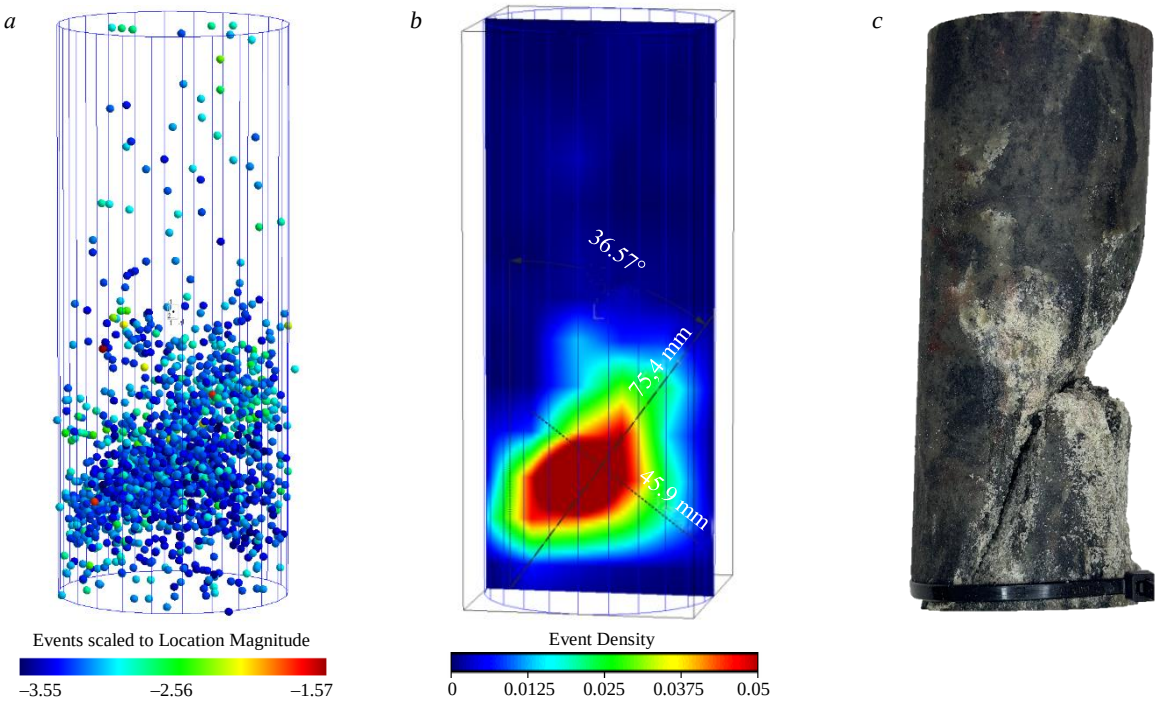


Fig.3. Analysis of the microcrack zone for metamorphic rocks (ore sample of a rich zone with a tensile strength of 208 MPa): *a* – distribution of hypocenters of AE events; *b* – density of AE events; *c* – sample after tests with an inclined macrofracture

For the ore sample of the rich zone (Fig.3), an increase in the event density to 0.1 events/mm^3 is observed. The assessment of the microcrack zone also indicates its increase (the ratio of the zone width to the length of the macrofracture is 0.609). At the same time, the angle β exceeds the range of angles predicted in [20] that satisfy brittle fracture and is equal to 36.57°, the *b*-factor is characterized by the highest value for urtites and ores of 1.73, which indicates a decrease in radiation energy.

This is an open access article under the CC BY 4.0 license

Table 3

Acoustic emission parameters

Rock sample	Comprehensive pressure σ_3, MPa	Pore pressure, MPa	Tensile strength, MPa	The maximum value of the AE *b*-factor	Exp-factor of AE	Maximum density of AE events, events/mm^3	The ratio of the size of the microcrack zone	The angle of inclination of the main crack β, degree
Massive urtites, coarse-grained, N8	40	–	523	0.64	0.0014	0.025	0.342	22.32
Massive urtites, coarse-grained, N1'	40	–	463	0.76	0.0015	0.025	0.316	20.44
Ores of the poor zone, fine-grained, N1	40	–	520	1.25	0.0027	0.05	0.223	21.23
Ores of the rich zone, fine-grained, N2	40	–	208	1.73	0.0032	0.1	0.609	36.57
Limestone, hidden fine-grained, DP22-2	50	30	329	2.09	–	–	–	0
Limestone, hidden fine-grained, DP21-2	75	30	304	1.73	–	–	–	0

Figure 4 shows the results of the analysis of the *b*-factor and AE activity for igneous and metamorphic rocks in the form of graphs of parameter changes during the tests, compared with loading curves. It can be seen that for igneous rocks (urtites), the approximation curves (black lines) are more flat compared to metamorphic ones (ores). This indicates the gradual formation of microcracks in urtites and accelerated formation in ores, which affects the increase in the exp-factor.

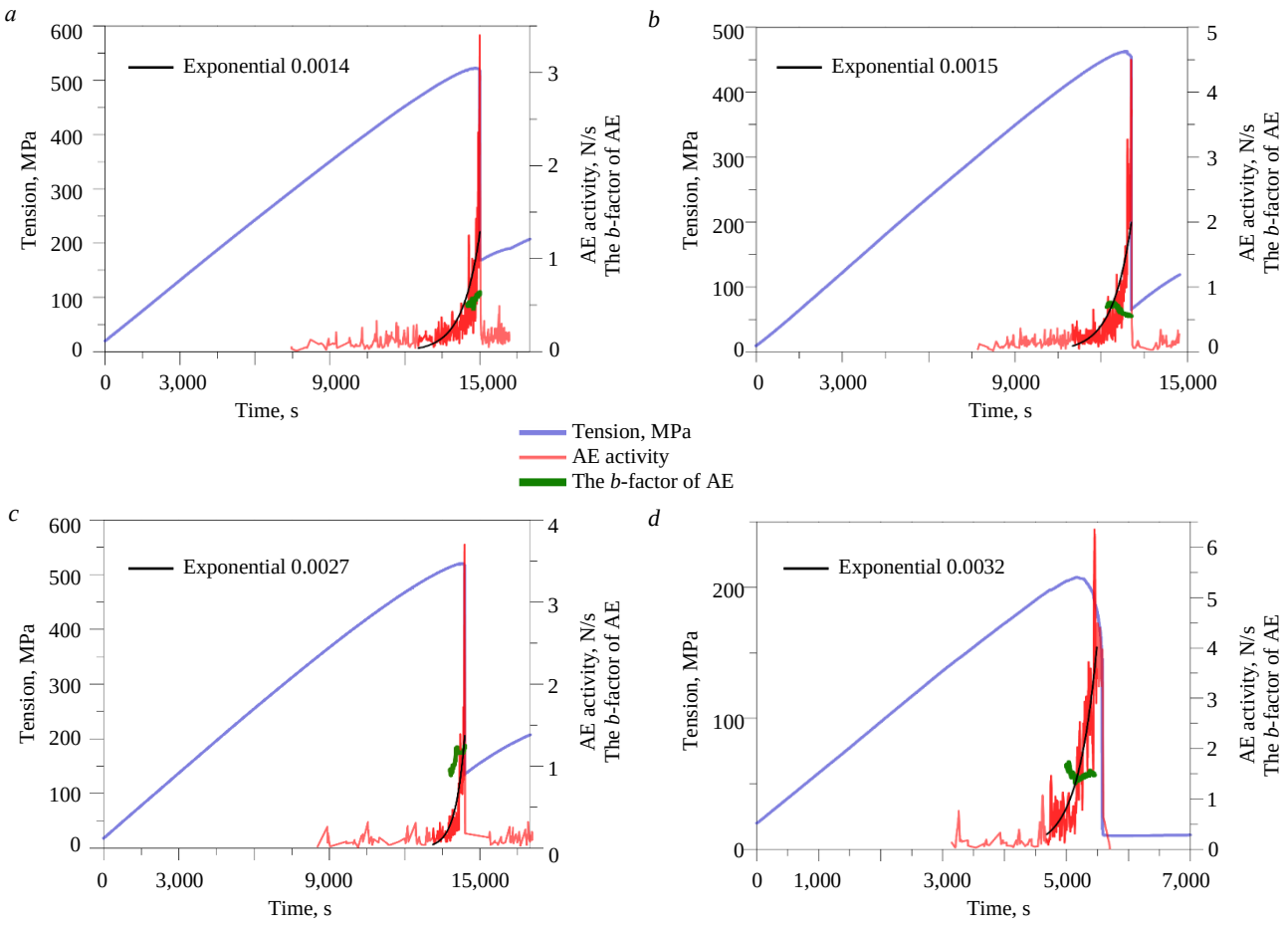


Fig.4. Analysis of AE and *b*-factor activity for igneous (urtites) and metamorphic (ores) rocks:
a – urtite sample with a tensile strength of 523 MPa; *b* – urtite sample with a tensile strength of 463 MPa;
c – poor zone ore sample with a tensile strength of 520 MPa; *d* – rich ore sample zones with a tensile strength of 208 MPa

This is an open access article under the CC BY 4.0 license

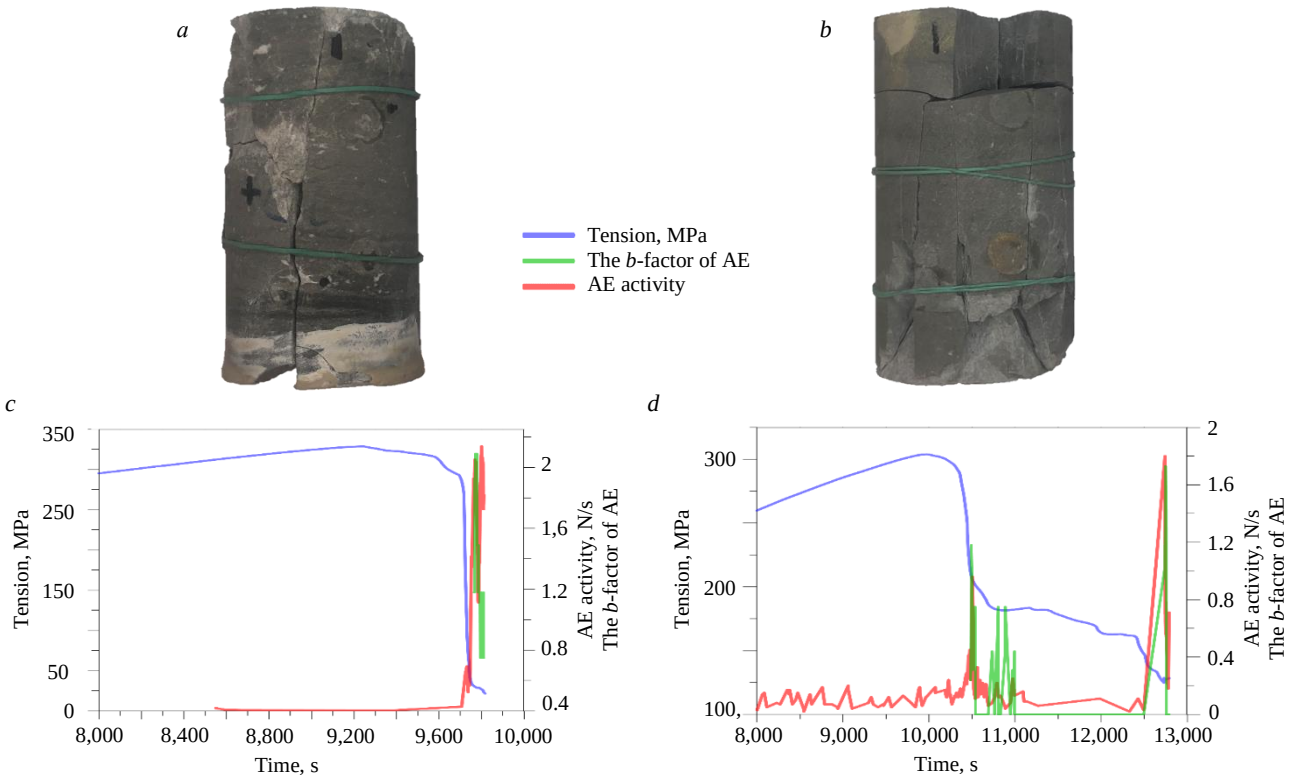


Fig.5. Analysis of AE and b-factor activity for sedimentary rocks:
a – limestone sample with a tensile strength of 329 MPa after testing (main vertical crack is visible);
b – limestone sample with a tensile strength of 304 MPa after testing (three main vertical cracks are visible);
c – the final stage of destruction of limestone with a tensile strength of 329 MPa;
d – the final stage of destruction of limestone with a tensile strength of 304 MPa

Figure 5 shows the results of the analysis of the *b*-factor and AE activity for sedimentary rocks (limestones) in the form of graphs of changes in these parameters during the tests, compared with loading curves. Photographs of samples after testing are also shown, which clearly show vertical mainline cracks. Thus, the fracture geometry differs significantly from igneous and metamorphic rocks. According to the activity trends, it can be seen that there are no precursors of destruction in the AE process, which indicates the absence of formation of a microcrack zone and, as a result, dilatancy, the *b*-factor has the maximum value among all the samples considered (2.09). All this indicates the extreme localization of the destruction process.

The spatial and temporal parameters of AE controlling the deformation process in rocks of various genesis are summarized in Table 3.

Figure 6 shows the average data of independent studies of the deformation process for four groups of rocks corresponding to the tested samples with AE registration. Only nonlinear loading sections corresponding to decompression are shown. Samples of sedimentary and metamorphic (poor ores) rocks exhibit a decompression effect at a ratio σ^p/σ_c^p equal to 0.53, igneous and metamorphic (rich ores) rocks at ratios of

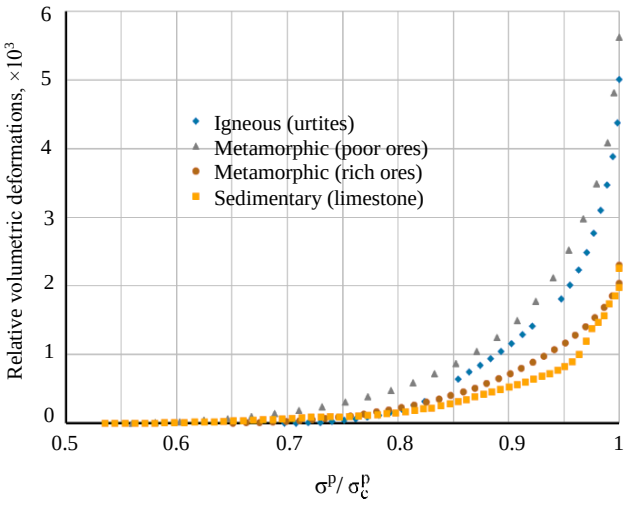


Fig.6. Graphs of the dependences of relative volumetric deformations on the ratio of acting differential stresses to the ultimate strength for the studied four groups of rocks

This is an open access article under the CC BY 4.0 license

0.70 and 0.65, respectively. It can be seen that for igneous (urtites) and metamorphic (poor ores) rocks, volumetric deformations are significantly greater than for rich ores and sedimentary (limestones) rocks. This result is in good agreement with the obtained AE parameters. Dilatancy is accompanied by an increase in volumetric deformation with a brittle fracture mechanism. Analysis of spatial and temporal parameters of AE (Table 3) showed that samples of igneous rocks and ores of the poor zone (metamorphic rocks) meet the criteria of brittle fracture. At the same time, the value of the microcrack zone is higher for igneous rocks (0.342 and 0.316) than for metamorphic rocks (0.223). This suggests that the microcracking zone for the ore of the poor zone is more localized. Thus, it can be concluded qualitatively that both types of rocks are characterized by the phenomenon of dilatancy.

In the ore of the rich zone, with the maximum index of the width of the microcrack zone (0.609) and the maximum density of events (0.1 events/mm^3) the angle β tends to 45° and equal to 36,57°, exceeds the range for brittle fracture [20], the *b*-factor acquires the maximum value (1.73) of those obtained for igneous (urtites) and metamorphic (ore) rocks. At the same time, the volumetric deformation for rich ore (Fig.6) is characterized by more than twice the value compared to urtites and poor ore. Hence, it is assumed that a lot of low-energy cracks are formed in a sample of rich ore, characterized by a lack of opening which indicates the predominance of plastic deformation and, as a result, a decrease in dilatancy. The resulting main crack develops in the form of a sliding platform.

An increase in the *b*-factor with an increase in the role of plastic deformation was noted in [29, 34], where AE parameters for rocks of various genesis were studied. When comparing the results of uniaxial loading of samples for Westerly granite, the maximum value of the *b*-factor turned out to be 1.68, for marble – 2.50.

For sedimentary rocks (limestones), there is an inverse change in the angle β compared to rich ores – the angle tends to zero. A joint consideration of this fact with the maximum value of the *b*-factor (2.09) leads to the conclusion about the maximum localization of the cracking process, i.e., about the minimum fracture zone. This, in turn, indicates the absence of dilatancy, which is confirmed by minimal volumetric deformation (Fig.6). The mechanism of formation of the resulting mainline cracks is similar to the Griffiths crack [35], which develops in the field of tensile stresses in an isotropic and homogeneous material.

Conclusion. The results of the performed complex of laboratory studies of the mechanism of destruction and the process of acoustic emission in rocks of different genesis under stress conditions corresponding to depths of up to 5 km, allow to conclude:

• Three types of macrofracture have been identified in rocks of different genesis: brittle fracture with the formation of a rock mass of layered cracks (in urtites and poor ores); brittle fracture with the formation of single vertical Griffiths-type cracks (in limestones); plastic deformation and fracture (in rich ores).

• In igneous (massive urtite) and metamorphic (apatite-nepheline ore) rocks, the phenomenon of dilatancy is observed with the formation of a network of communicating separation cracks, which determines the possibility of formation of fractured reservoirs in the rock mass at deep depths. To a greater extent, dilatancy manifests itself in massive urtites and forms a developed microcracking zone. Both spatial and temporal localization of the microcracking process is observed in apatite-nepheline ores.

• In limestones, there is an extreme case of localization of the microcracking process, and dilatancy in them is close to zero. This corresponds to the model proposed by Z.Rechs and D.Lochner, on the origin and growth of faults in brittle rocks, showing that as the ratio of the distance between cracks to the size of cracks tends to zero (localization of the process), the angle of inclination β also tends to zero. This is confirmed by testing limestone samples with pore pressure, where there was no filtration, which manifested itself only at the final stage of macrofracturing during the formation of single vertical cracks.

This is an open access article under the CC BY 4.0 license

• From the point of view of parameterization of acoustic emission, it is necessary to supplement the *b*-factor studies with an analysis of the AE source function for each event characterizing the kinematics of the germination of a single crack, which will make it possible to determine the scale of the microcrack zone in various rocks, as well as the criterion for the transition from one level of fracture to another.

• The results of petrographic analysis of rock samples before and after the test may be a factor confirming the assumption that increased values of the *b*-factor can be used to judge a decrease in the size of cracks formed in rocks of different genesis.

REFERENCES

1. Lockner D.A., Byerlee J.D., Kuksenko V. et al. Chapter 1. Observations of Quasistatic Fault Growth from Acoustic Emissions. Fault Mechanics and Transport Properties of Rocks. Academic Press, 1992, p. 3-31. DOI: 10.1016/S0074-6142(08)62813-2

2. Lockner D.A., Byerlee J.D., Kuksenko V. et al. Quasi-static fault growth and shear fracture energy in granite. *Nature*. 1991. Vol. 350. N 6313, p. 39-42. DOI: 10.1038/350039a0

3. Kuksenko V., Tomilin N., Damaskinskaya E., Lockner D. A two-stage model of fracture of rocks. *Pure and Applied Geophysics*. 1996. Vol. 146. N 2, p. 253-263. DOI: 10.1007/BF00876492

4. Prischepa O.M., Kireev S.B., Nefedov Yu.V. et al. Theoretical and methodological approaches to identifying deep accumulations of oil and gas in oil and gas basins of the Russian Federation. *Frontiers in Earth Science*. 2023. Vol. 11. N 1192051. DOI: 10.3389/feart.2023.1192051

5. Egorov A.S., Prischepa O.M., Nefedov Y.V. et al. Deep Structure, Tectonics and Petroleum Potential of the Western Sector of the Russian Arctic. *Journal of Marine Science and Engineering*. 2021. Vol. 9. Iss. 3. N 258. DOI: 10.3390/jmse9030258

6. Ilyinov M.D., Petrov D.N., Karmanskiy D.A., Selikhov A.A. Physical simulation aspects of structural changes in rock samples under thermobaric conditions at great depths. *Mining Science and Technology*. 2023. Vol. 8. N 4, p. 290-302. DOI: 10.17073/2500-0632-2023-09-150

7. Korshunov V.A., Pavlovich A.A., Bazhukov A.A. Evaluation of the shear strength of rocks by cracks based on the results of testing samples with spherical indentors. *Journal of Mining Institute.* 2023. Vol. 262, p. 606-618. DOI: 10.31897/PMI.2023.16

8. Verbilo P., Karasev M., Belyakov N., Iovlev G. Experimental and numerical research of the jointed rock mass anisotropy in three-dimensional stress field. *The Mining-Geology-Petroleum Engineering Bulletin*. 2022. Vol. 37. N 2, p. 109-122. DOI: 10.17794/rgn.2022.2.10

9. Xiao-Ping Zhang, Louis Ngai Yuen Wong. Cracking Processes in Rock-Like Material Containing a Single Flaw Under Uniaxial Compression: A Numerical Study Based on Parallel Bonded-Particle Model Approach. *Rock Mechanics and Rock Engineering*. 2012. Vol. 45. Iss. 5, p. 711-737. DOI: 10.1007/s00603-011-0176-z

10. Xiao-Ping Zhang, Louis Ngai Yuen Wong. Crack Initiation, Propagation and Coalescence in Rock-Like Material Containing Two Flaws: a Numerical Study Based on Bonded-Particle Model Approach. *Rock Mechanics and Rock Engineering*. 2013. Vol. 46. Iss. 5, p. 1001-1021. DOI: 10.1007/s00603-011-0176-z

11. Ilyinov M.D., Kartashov Yu.M., Karmanskii A.T., Kozlov V.A. Influence of rock disturbance on their rheological properties. *Journal of Mining Institute.* 2010. Vol. 185, p. 31-36 (in Russian).

12. Ilinov M.D., Kartashov Yu.M. Qiuck-acting technique for the determination of rheological properties of rocks. *Journal of Mining Institute.* 2011. Vol. 190, p. 207-209 (in Russian).

13. Davis R.O., Selvadurai A.P.S. Plasticity and Geomechanics. Cambridge University Press, 2002, p. 300. DOI: 10.1017/CBO9780511614958

14. Kuksenko V.S., Makhmudov K.F., Mansurov V.A. et al. Changes in structure of natural heterogenous materials under deformation. *Journal of Mining Science.* 2009. Vol. 45. Iss. 4, p. 355-358. DOI: 10.1007/s10913-009-0044-3

15. Trushko V.L., Protosenya A.G. Prospects of Geomechanics Development in the Context of New Technological Paradigm. *Journal of Mining Institute.* 2019. Vol. 236, p. 162-166. DOI:10.31897/PMI.2019.2.162

16. Grishchenko A.I., Semenov A.S., Melnikov B.E. Modeling the processes of deformation and destruction of the rock sample during its extraction from great depths. *Journal of Mining Institute.* 2021. Vol. 248, p. 243-252. DOI: 10.31897/PMI.2021.2.8

17. Rasskazov I.Yu., Cirel S.V., Rozanov A.O. et al. Application of Acoustic Measurement Data to Characterize Initiation and Development of Disintegration Focus in a Rock Mass. *Journal of Mining Science.* 2017. Vol. 53. N 2, p. 224-231. DOI: 10.1134/S1062739117022055

18. Jie Li, Mingyang Wang, Kaiwen Xia et al. Time-dependent dilatancy for brittle rocks. *Journal of Rock Mechanics and Geotechnical Engineering*. 2017. Vol. 9. Iss. 6. P. 1054-1070. DOI: 10.1016/j.jrmge.2017.08.002

19. LianYing Zhang, XianBiao Mao, AiHong Lu. Experimental study on the mechanical properties of rocks at high temperature. Science in China Series E: Technological Sciences. 2009. Vol. 52. Iss. 3, p. 641-646. DOI: 10.1007/s11431-009-0063-y

20. Reches Z., Lockner D.A. Nucleation and growth of faults in brittle rocks. *Journal of Geophysical Research: Solid Earth*. 1994. Vol. 99. Iss. B9, p. 18159-18173. DOI: 10.1029/94JB00115

21. Zang A., Wagner C., Stanchits S. et al. Fracture process zone in granite. *Journal of Geophysical Research: Solid Earth*. 2000. Vol. 105. Iss. B10, p. 23651-23661. DOI: 10.1029/2000JB900239

22. Zang A., Wagner C.F., Dresen G. Acoustic emission, microstructure, and damage model of dry and wet sandstone stressed to failure. *Journal of Geophysical Research: Solid Earth*. 1996. Vol. 101. Iss. B8. P. 17507-17521. DOI: 10.1029/96jb01189

This is an open access article under the CC BY 4.0 license

23. Baud P., Klein E., Wong T.-f. Compaction localization in porous sandstones: spatial evolution of damage and acoustic emission activity. *Journal of Structural Geology*. 2004. Vol. 26. Iss. 4, p. 603-624. DOI: 10.1016/j.jsg.2003.09.002

24. S.-H. Chang, C.-I. Lee. Estimation of cracking and damage mechanisms in rock under triaxial compression by moment tensor analysis of acoustic emission. *International Journal of Rock Mechanics and Mining Sciences*. 2004. Vol. 41. Iss. 7, p. 1069-1086. DOI: 10.1016/j.ijrmms.2004.04.006

25. Karmansky A.T. Collecting properties of rocks in changes of stress state type. *Journal of Mining Institute*. 2009. Vol. 183, p. 289-292 (in Russian).

26. Pollard D.D., Segall P. 8 – Theoretical displacements and stresses near fractures in rock: with applications to faults, joints, veins, dikes, and solution surfaces. Fracture Mechanics of Rock. Academic Press, 1987, p. 277-349. DOI: 10.1016/B978-0-12-066266-1.50013-2

27. Hofmann H., Babadagli T., Jeoung Seok Yoon et al. A grain based modeling study of mineralogical factors affecting strength, elastic behavior and micro fracture development during compression tests in granites. *Engineering Fracture Mechanics*. 2015. Vol. 147, p. 261-275. DOI: 10.1016/j.engfracmech.2015.09.008

28. Pozhilenko V.I., Gavrilenko B.V., Zhirov D.V., Zhabin S.V. Geology of mineral areas of the Murmansk Region. Apatity: Kola Science Centre RAS, 2002, p. 359 (in Russian).

29. Scholz C.H. The frequency-magnitude relation of microfracturing in rock and its relation to earthquakes. *Bulletin of the Seismological Society of America*. 1968. Vol. 58. N 1, p. 399-415. DOI: 10.1785/BSSA0580010399

30. Wyss M. Towards a Physical Understanding of the Earthquake Frequency Distribution. *Geophysical Journal of the Royal Astronomical Society*. 1973. Vol. 31. Iss. 4, p. 341-359. DOI: 10.1111/j.1365-246X.1973.tb06506.x

31. Zuhair Hasan El-Isa. Frequency-Magnitude Distribution of Earthquakes. Earthquakes – Forecast, Prognosis and Earthquake Resistant Construction. IntechOpen, 2018, p. 87-107. DOI: 10.5772/intechopen.77294

32. Zang A., Stanchits S., Dresen G. Acoustic Emission Controlled Triaxial Rock Fracture and Friction Tests. Proceedings of the International Conference on Structural Integrity and Fracture, 25-27 September 2002, Perth, Australia. A.A. Balkema Publishers, 2002, p. 289-296.

33. Malén K., Bolín L. A Theoretical Estimate of Acoustic-Emission Stress Amplitudes. *Physica Status Solidi* (*B*). 1974. Vol. 61. N 2, p. 637-645. DOI: 10.1515/9783112502020-030

34. Scholz C.H. Microfracturing and the inelastic deformation of rock in compression. *Journal of Geophysical Research*. 1968. Vol. 73. Iss. 4, p. 1417-1432. DOI: 10.1029/JB073i004p01417

35. Griffith A.A. The Phenomena of Rupture and Flow in Solids. Philosophical Transactions of the Royal Society of London. Series A, Containing Papers of a Mathematical or Physical Character. 1921. Vol. 221. Iss. 582-593, p. 163-198. DOI: 10.1098/rsta.1921.0006

***Authors*: Vladimir L. Trushko,** *Doctor of Engineering Sciences*, *Director of the Institute of Special Scientific Projects*, *Trushko_VL@pers.spmi.ru*, *https://orcid.org/0000-0002-9742-1076* (*Empress Catherine II Saint Petersburg Mining University*, *Saint Petersburg*, *Russia*), **Aleksandr O. Rozanov,** *Senior Researcher*, *https://orcid.org/0009-0006-4615-0401* (*Empress Catherine II Saint Petersburg Mining University*, *Saint Petersburg*, *Russia*), **Malik M. Saitgaleev,** *Postgraduate Student*, *https://orcid.org/0000-0002-9859-5799* (*Empress Catherine II Saint Petersburg Mining University*, *Saint Petersburg*, *Russia*), **Dmitrii N. Petrov,** *Candidate of Engineering Sciences*, *Associate Professor*, *https://orcid.org/0000-0002-5513-1871* (*Empress Catherine II Saint Petersburg Mining University*, *Saint Petersburg*, *Russia*), **Mikhail D. Ilinov,** *Candidate of Engineering Sciences*, *Head of the Laboratory*, *https://orcid.org/0009-0007-2185-8638* (*Empress Catherine II Saint Petersburg Mining University*, *Saint Petersburg*, *Russia*), **Daniil A. Karmanskii,** *Leading Engineer*, *https://orcid.org/0000-0002-3214-5322* (*Empress Catherine II Saint Petersburg Mining University*, *Saint Petersburg*, *Russia*), **Aleksandr A. Selikhov,** *Postgraduate Student*, *https://orcid.org/0009-0005-8163-2249* (*Empress Catherine II Saint Petersburg Mining University*, *Saint Petersburg*, *Russia*).

The authors declare no conflict of interests.

This is an open access article under the CC BY 4.0 license